TEMPERATURE DEPENDENT RAMAN SPECTROSCOPY OF MoS_2 MONOLAYER

DISSERTATION

SUBMITTED TO
DEPARTMENT OF PHYSICS
SCHOOL OF PHYSICAL SCIENCES
DOON UNIVERSITY, DEHRADUN

IN THE PARTIAL FULFILMENT OF THE
REQUIREMNETS OF THE DEGREE OF

MASTER IN PHYSICS

BY

MONIKA BISHT (17PH-12)

DEPARTMENT OF PHYSICS
SCHOOL OF PHYSICAL SCIENCES
DOON UNIVERSITY, DEHRADUN
UTTARAKHAND (INDIA)
2022

Declaration

I declare that the work presented in the Dissertation entitled **"Temperature dependent Raman Spectroscopy of MoS_2 Monolayer"** synthesized by Chemical Vapour Deposition method' being submitted to the Department of Physics, School of Physical Sciences, Doon University, Dehradun for the award of Master in Physics is my original research work.

The Dissertation embodies the results of investigations, observations, and experiments carriedout by me. I have neither plagiarized any part of the dissertation nor have submitted same work for the award of any other degree/diploma anywhere.

Monika Bisht

17PH-12

Date: 30 / 07 / 2022

Certificate

This is to certify that Dissertation entitle **"Temperature dependent Raman spectroscopy of MoS_2 monolayer"** is submitted by Monika Bisht and has been done under my supervision. It is also certified that the work in this Dissertation embodies original research and hard work of the candidate. The assistance and support received during the course of investigation and all the Sources of literature have been fully acknowledged.

Supervisor/Guide
Dr. Himani Sharma
Assistant Professor
Department of Physics
School of Physical science
Doon University

Head of Department
Dr. Himani Sharma
HOD In Charge
Department of Physics
School of Physical Sciences
Doon University

Acknowledgment

I express my deep gratitude to my project supervisor Dr. Himani Sharma for providing me with the opportunity to work under her supervision and encourage, motivated, supported and provided me such an informative environment during my project work. Her constant assistance and guidance helped me and encouraged me tackling the obstacles and led to develop a positive attitude and appreciation for the subject.

I would like to express my deep gratitude to research scholars Saurabh Rawat and Dr. Priyanka Bamola for their constant support and assistance throughout the project. They worked very hard throughout in introducing us to the lab equipment, apparatuses, machines and their workings. Their constant push and assistance in understanding the concepts and mechanisms had only led to the successful completion of project on time. They developed a good interaction with me along with everybody else and appreciated to ask doubts and helped clearing the doubts regarding any operations of machines and working of required computer applications. They constantly monitored our work and insisted to maintain discipline, cleanliness, and take necessary precaution while operating equipment.

I would also like to thank Dr. Rajesh sir of department Physics from IIT Indore for their constant guidance.

Secondly, I would like to express my sincere appreciation to my lab-mates and colleagues Shreya Negi, Bhuvan Bhandari, Deepali Aswal, Abhinav Bhatt and Stuti Dhpola for their cooperation and creating a healthy atmosphere during the course of project. Their collective problem discussing attitude and assistance had been quite helpful.

Monika bisht

17PH-12

Abstract

The effect of thermal perturbations on different Raman active phonon modes has been studied using temperature dependent Raman spectroscopy of MoS_2. The MoS_2 nanosheet was prepared using Chemical vapour deposition (CVD) and characterized using Scanning electron microscopy (SEM), X-ray diffraction(X-RD), X-ray photoelectron spectroscopy (XPS), and Raman spectroscopy. Raman spectra recorded at temperatures higher than room temperature (300K-573K) and below room temperature (198K-300K) were analyzed using the theoretical framework developed by taking hot phonon anharmonicity into account. Temperature-dependent responses for E^1_{2g} , A_{1g} 2LA(M) modes were observed in Origin. The laboratory results revealed that phonon–phonon interaction and electron phonon interaction play a dominating role in broadenings and shifting of peaks at different temperature range. The E^1_{2g}, A_{1g} and 2LA(M) Raman active modes, confirming the anharmonic effect's.

The temperature-dependent red shift in peak location and widening of the Raman modes $E^1_{2g,}$ A_{1g} and 2LA(M) with respect to room temperature below and above (298k) tells us about increases in crystallinity of material. The behavior of phonons under the effect of increased temperatures has been presented in detail, with good agreement between experimental and theoretical frameworks. And according to literature we calculate temperature coefficient for each Raman modes E^1_{2g} (- 0.01808 cm^{-1}/K), A_{1g} (-0.01581cm^{-1}/K) and 2LA(M) (-0.01856 cm^{-1}/K). From literature review and experimental data analysis the calculated negative temperature coefficient have application for photo electronic devices.

Contents

List of Figures

LIST OF TABELS

List of Abbreviation's

2D- Two-dimensional

TMDCs/TMDs- Transition Metal Dichalcogenides

MoS_2 - Molybdenum Disulfide

XPS- X-ray Photoelectron Spectroscopy

CVD- Chemical Vapor Deposition

SiO_2- Silicon Dioxide

S- Sulfur

Mo- Molybdenum

FET- Field-Effect Transistor

Si- Silicon

XRD- X-Ray Diffraction

SEM- Scanning Electron Microscope

λ- Wavelength

Θ- Angle of incidence

DI- De-Ionized

MoO_3- Molybdenum Trioxide

FWHM-Full width at half maxima

Chapter-1

Introduction

Recently, two-dimensional materials like graphene have gained attention because of their exceptional electrical and optical properties. The first two-dimensional material synthesized was graphene, it is one atom thick [1]. Graphene has no band gap As its valence band and conduction band touch, it is also considered as semi-metal[2]. With similar qualities to graphene and to deal with the drawbacks of the zero bandgap [2], 2D TMDs were discovered as the ideal substitute for graphene. Due to their band gap qualities between 1-2 eV, 2D TMDs, semiconductor materials with distinct properties like electrical, mechanical, and optical properties,[3] appeared to be extremely promising for usage in next-generation semiconductor devices. MoS_2 is a typical TMDC that has gained widespread study interest because to its fascinating properties. Like, Tunable band gap[4], rapid carrier dynamics, outstanding electroluminescence and photoluminescence [5] characteristics, and so on distinguish two-dimensional MoS_2.

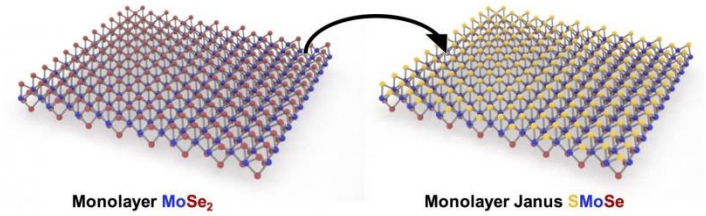

Fig 1.1: 2-D material structure

Source: 2-faced 2-D material is a first at Rice (14 August 2017)

1.2 TMDCs (Transition Metal Dichalcogenides)

TMDCs are atomically thin semiconductors. Having general formula of the MX_2 where M is a transition metal atom and X is a chalogens atom [6] shown in fig 1.2.. A layer of M atoms is sandwiched between two layers of X atoms. The metal can have either trigonal prismatic or octahedral coordination [7]. TMDCs have electronic properties ranging from semiconducting (n-type, p-type) to superconducting depending upon chemical composition.

Group-VI TMDCs monolayers (e.g., MoS_2, WS_2, $MoSe_2$, and WSe_2) exhibit semiconductor behavior.

Recently TMDCs have drawn attention in many fields after the discovery of graphene and wide applications 2D nanomaterials in many fields.

(A)

IA																	0
1 H	IIA											IIIA	IVA	VA	VIA	VIIA	2 He
3 Li	4 Be											5 B	6 C	7 N	8 O	9 F	10 Ne
11 Na	12 Mg	IIIB	IVB	VB	VIB	VIIB	VIII			I B	II B	13 Al	14 Si	15 P	16 S	17 Cl	18 Ar
19 K	20 Ca	21 Sc	22 Ti	23 V	24 Cr	25 Mn	26 Fe	27 Co	28 Ni	29 Cu	30 Zn	31 Ga	32 Ge	33 As	34 Se	35 Br	36 Kr
37 Rb	38 Sr	39 Y	40 Zr	41 Nb	42 Mo	43 Tc	44 Ru	45 Rh	46 Pd	47 Ag	48 Cd	49 In	50 Sn	51 Sb	52 Te	53 I	54 Xe
55 Cs	56 Ba	La-Lu	72 Hf	73 Ta	74 W	75 Re	76 Os	77 Ir	78 Pt	79 Au	80 Hg	81 Tl	82 Pb	83 Bi	84 Po	85 At	86 Rn
87 Fr	88 Ra	Ac-Lr	104 Rf	105 Db	106 Sg	107 Bh	108 Hs	109 Mt	110 Ds	111 Rg	112 Cn	113 Uut	114 Uuq	115 Uup	116 Uuh	117 Uus	118 Uuo

Fig 1.2 Periodic table where red is transition metals and yellow is chalogens
Source:* *https://doi.org/10.1002/inf2.12161

1.3 Molybdenum disulfide (MoS_2)

An organic substance made of Molybdenum and Sulphur is known as Molybdenum disulfide (MoS_2).It is a naturally occurring, silvery black solid called Molybedite with a hexagonally layered structure. The semiconductor has a direct band gap of 1.8 eV(bulk) and an indirect band gap of 1.2 eV (monolayer)[8]. MoS_2 typically has a laminar S-Mo-S structure in just one layer. In a single layer of MoS_2, the Mo atom is sandwiched between two S atoms, or S-Mo-S. In a trigonal prismatic D_{3h} space group 6, the Mo atoms of MoS_2 have a coordination of six, whereas the sulphur atoms have a coordination of three[9]. The electrical properties can be controlled in part by the coordination of the Mo metal and its d-electrons.

1.3.1 Crystal Structure of MoS_2

The coordination phase of MoS_2 is either trigonal prismatic (2H) or octahedral (1T) exists in a single layer. In phases 1T, 2H, and 3R, the letter denotes the type of symmetry and the

number denotes the number of layers in the crystallographic unit cell. Tetragonal, hexagonal, and rhombohedra is the letters T, H, and R, respectively. (*J. Mex. Chem. Soc.* **2019)**.

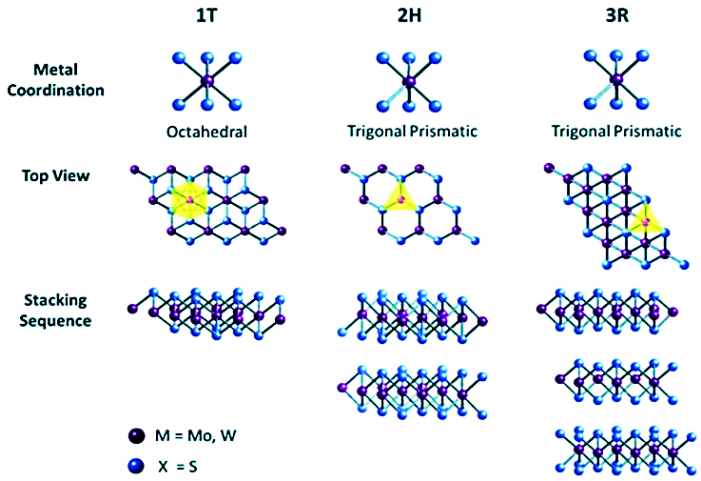

Fig 1.3 crystal structure for MoS_2 phases
Source:* *https://doi.org/10.3390/cryst11040355

1T-MoS_2 is a metastable crystalline phase having tetragonal symmetry and is metallic. 1T- MoS_2 monolayer is a slab of hexagonal Mo lattice occupies at the center by octahedral coordination between two layers of hexagonally packed S atoms. In both 2H-MoS_2 and 3R- MoS_2 phases each Mo atom is covalently bonded to six surrounding S atoms forming a trigonalprismatic coordination.

2H molybdenum disulfide (MoS2) is one of the transition metal Dichalcogenides that has received the most attention over the past few decades. It is the stable hexagonal phase of. The metastable phases of MoS2 (1T, 1T′, 1T″, and 1T‴) have had a resurgence in interest over the past five years. These metastable phases are made up of edge-sharing [MoS_6] octahedral, in contrast to the edge-sharing [MoS_6] trigonal prisms in the 2H MoS_2 phase, where the surrounding Mo-Mo distances diverge. These metastable polytypes are endowed with intriguing physical properties and have potential applications in a variety of sectors because of the numerous crystal structures and electronic configurations of the [MoS6] motifs that make them up. The most recent developments in metastable MoS_2 research are outlined in this review, with a focus on the various synthetic techniques.[10] .

3R-MoS_2 (rhombohedral), due to its thermal stability, ABC stacking (as opposed to the AA′ of the more prevalent 2H-MoS_2), and absence of inversion symmetry, the 3R-MoS_2 (rhombohedral) phase has garnered the greatest attention. It is a great contender for photonics, optoelectronics, and catalysis because of these qualities. This review aims to summarized 3R-history, MoS_2's known and predicted properties, syntheses, applications, and common misconceptions because the body of literature on it is quickly growing.[11]

The bandgap of single layer 2H-MoS_2 is found to be double than that of bulk 3R-MoS_2.[12].

2H- MoS_2 phase is more stable at high temperature as compared to 3R-MoS_2. [13]

1.1 Properties of Molybdenum Di-Sulfide

Table 1.1 Properties of MoS_2

Chemical Formula	MoS_2
Band gap	1.23 eV (direct, bulk) 1.8 eV (indirect, monolayer)
Molar mass	160.7 g mol^{-1}
Density	5.06 g cm^{-3}
Melting point	1185^0 C
Solubility	Insoluble in water

In bulk form, the weak interlayer interactions allows sheets to easily slide over one-another, so it is often used as lubricant. [14]

The optical bandgap transforms from indirect to direct one when the dimensions of MoS_2 is reduced from bulk to monolayer sheet. The indirect band gap become larger while the number of layered decreases due to quantum confinement effect in c-axis direction.[15] This unique bandgapproperties lead to better application in opto-electronic devices.

Semiconductor nature of MoS_2 can determine optically active in visible region.[16]

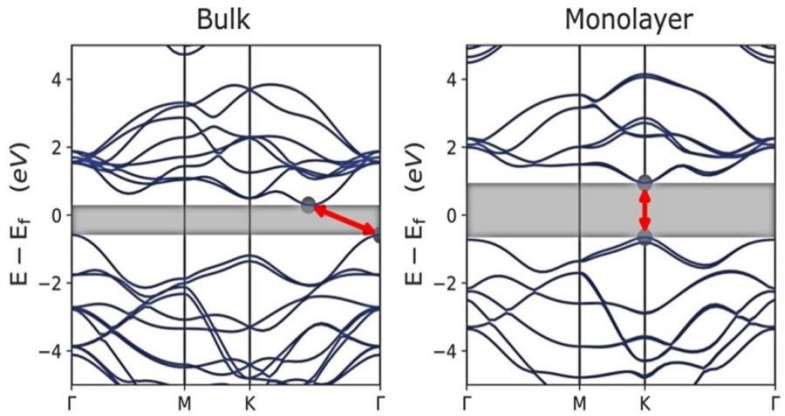

Figure 1.4 Represent Band diagram of bulk and monolayer MoS2 showing crossover from indirect to direct bandgap accompanied by a widening of the bandgap.

Source: Molybdenum Disulfide, MoS_2: Theory, Structure & Applications

1.6 Application of MoS_2:

1.6.1 FETs (Field Effect Transistor):

MoS_2 is n-channel FET's as it is n-type semiconductor. Since mobility of electrons is more therefore n-channel is a best FET's. FET MoS_2 has unique properties towards FETs due to its substantial direct bandgap and comparatively high carrier mobility. Single-layer MoS_2 transistors were the subject of early studies that showed significance, with high motilities and a good on/off ratio[17].

1.6.2 Photo Electronic Device:

Photo electronic devices generate voltage and current, when exposed in visible, infrared, or ultraviolet radiation. MoS_2 monolayer is optically active in visible region; it can be used in photo electronic devices such as LED's, Solar cells etc The MoS_2 photo electronic memory exhibits excellent memory characteristics, including a large programming/erasing current ratio that exceeds 10^7[18].

1.6.3 Lubricants:

Molybdenum disulfide is largely used as lubricants because of its layered structure and the materials can shear more easily parallel to these layers. The current usage of MoS_2 for

lubrication in spaceflight and dry machining, as well as anti-adhesive uses in extruding and moulding, are described. The state-of-the-art for modifying MoS_2 films currently involves adding dopants (co-sputtering), multilayering as a collection of films, each performing a particular function, or stacking repetitive nanometer-scale films.[19]

1.6.4 Gas Sensors:

The development of new semiconductor materials is still a major area of research due to the ongoing expansion of technological applications. New substances like molybdenum disulfide have been investigated recently as alternatives to silicon and graphene. One of the promising 2D materials with a direct bandgap, monolayer molybdenum disulfide (MoS_2), has a lot of potential for use in Nano electrical devices, energy storage, photo catalysts and chemical sensors. As a result, this research evaluates the current MoS_2 gas-sensing applications and compares them to those of other nanomaterials.[20]

1.5 Objective of thesis:

Based on above studies we took MoS_2 for our further studies (thesis). The objective of this thesis is to systematically establish, understand and optimize the chemical vapor deposition (CVD) and studying its temperature dependent Raman spectroscopy for MoS_2 monolayer.

CHAPTER-2

Synthesis and Characterization Techniques

In this chapter the several ways to create MoS_2 monolayers are briefly discussed. There are two different ways to create nanostructures: top-down and bottom-up. Although top-down methods are well developed, bottom-up methods are preferable because they have a higher likelihood of developing nanostructures with fewer flaws, more uniform chemical compositions, and the ability to produce smaller structures.

2.1 Top-Down Approaches

The top-down synthesis process creates nanostructures by etching out crystal planes that are already present on the substrate. It ensures consistency in particle size, shape, and geometry.

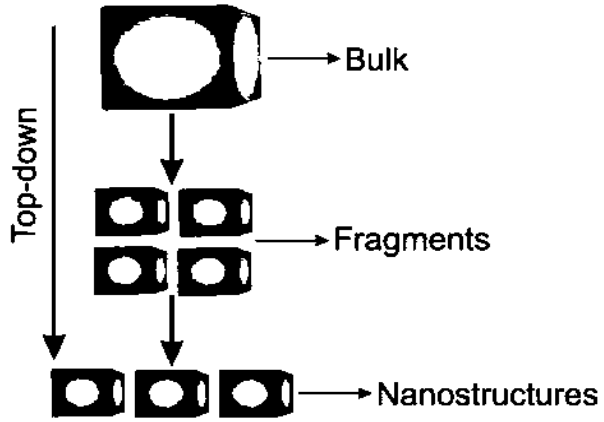

Figure 2.1 Representation of top-down approach for synthesis of nanomaterials
Source: https://doi.org/10.3390/chemosensors6020016

2.1.1 Micromechanical Exfoliation

Micromechanical exfoliation is simplest method and makes use of weak vdW forces. A scotch tape is used to peel off the layers of MoS_2 from bulk material. The tape is then pressed onto a substrate. The peeled off layer is transferred onto the substrate by vdW forces between them[21]. The disadvantage of this method is its limitation to lab scale.

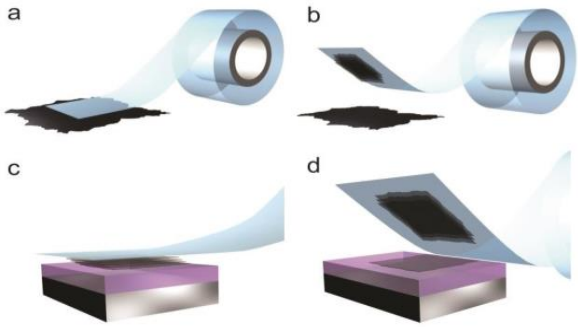

Figure 2.2 (a) Scotch tape pressed on bulk crystal, (b) Scotch tape peeled off Bringing multiple atomic layers with it, (c) Multilayers pressed onto desired substrate and (d) Tape peeled off again, leaving a single atomic monolayer behind.(Novoselov & Castro Neto, 2012)
Source: https://doi: 10.3740/MRSK.2017.27.12.705

2.1.2 Liquid Exfoliation:

Mechanical exfoliation can produce large-scaled, single-layered TMDC's that are flawless but have limitations. Chemical exfoliation has therefore been developed for the high yield and large-scale manufacture of TMDC nano-sheets in solution phase. Bulk MoS_2 in liquid phase exfoliation create flakes of arbitrary size and shape. Several methods, including mechanical exfoliation, chemical vapour deposition, and chemical exfoliations, have been used to create 2D-TMDCs. Chemical exfoliations, such as liquid-phase and intercalation isolations of TMDCs, are seen as potential options for high yield, remarkable performance, low cost, and exceptional up-scalability among cutting-edge synthetic methods.[22]

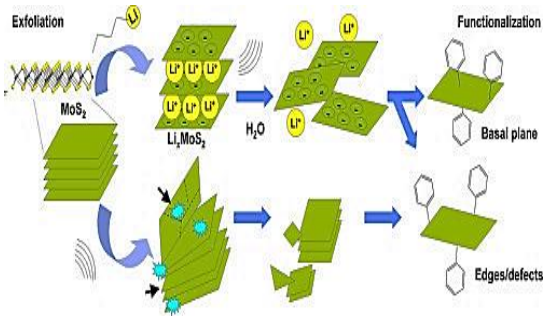

Figure 2.3 Production of MoS2 Nano sheets in isopropanol by a salt assisted direct liquid exfoliation.
Source: Production of mono- to few-layer MoS_2 nanosheet in isopropanol by a salt-assisted direct liquid-phase exfoliation method – Science Direct.

There are two ways to exfoliate MoS_2 in liquid.

1) The first is mechanical exfoliation using techniques like sonication, shearing and grinding.

2) The second is an electrochemical method called atomic intercalation.

2.2 Bottom-Up Approach:

A bottom-up approach implies the nanostructures are synthesized onto the substrate by stacking atoms onto each other which give rise to crystal planes, crystal planes further stack onto each other, resulting in formation of nanostructures. This approach is advantageous than the former in many aspects be it size constraints, etc.

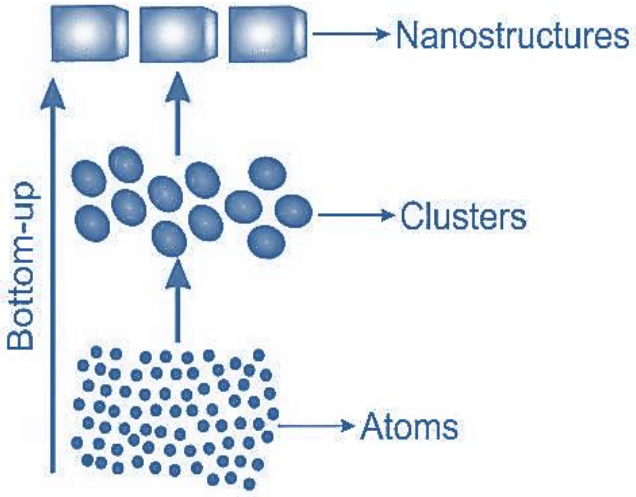

Figure 2.4 Representation of bottom-up approach for synthesis of nanomaterials
Source: https://doi.org/10.3390/chemosensors6020016

2.2.1 Physical Vapor Deposition (PVD)

Physical vapour deposition is a vaporization coating technique in which the material goes from a condensed phase to a vaporphase and then back to a thin film condensed phase. The most common form of physical vapor deposition is thermal evaporation, magnetron sputtering,(Kurapov et al., 2021) and arc vapor deposition.

The process involves four steps:

1) Evaporations of the material to be deposited.

2) Transport of the vapor to the substrate to be coated.

3) Reaction between metal andrespective reactive gas during transport.

4) Deposition of coating at substrate surface.

2.2.2 Chemical Vapor Deposition (CVD):

Chemical vapor deposition is a process in which volatile precursors are heated and then reacts chemically in vapor/gas to form the desired product which deposits over the substrate. CVD is a popularly used technique for 2D nanomaterials fabrication such as graphene, TMDCs.

It is an excellent fabrication method used vastly to synthesize controlled layer of MoS_2 and other 2D materials such as graphene, borophene, etc[25]. By varying the synthesis condition (temperature, pressure, concentration) the diameter, crystallinity and other morphology of the product can be controlled.

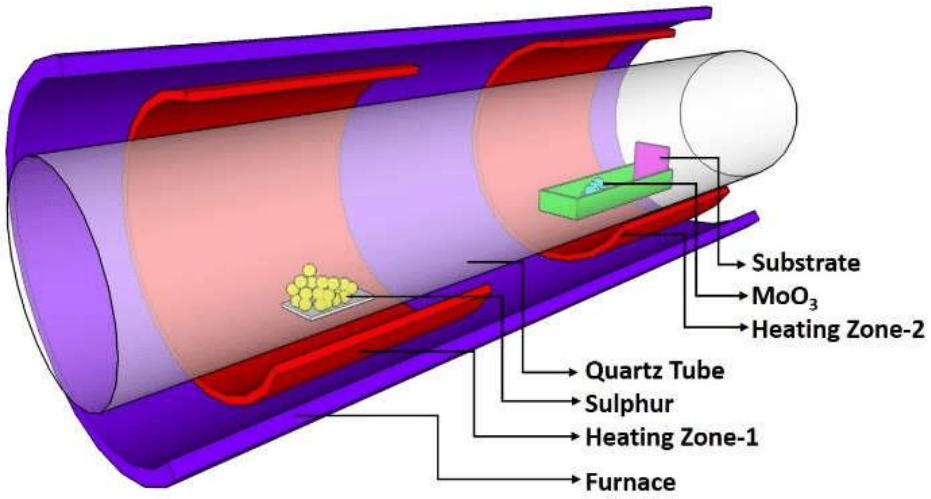

Figure 2.5 Represent inner-structure of CVD
Source: https://doi:10.1039/C8NR10092F

Steps involved during the CVD synthesis process:

1) Evaporation of precursor
2) Reaction of precursor and form new compound
3) Diffusion of the product on the substrate
4) Surface reaction leads to formation of film
5) CVD can categorize into various types based on the different ongoing processes

2.2.3 Solution Chemical Process

Hydrothermal synthesis and solvothermal synthesis typically use molybedite to react with sulfide or just sulfur in a stainless steel autoclave, where a series of physicochemical reactions take place under relatively high temperature (e.g., 200° C) and high pressure for several hours or longer. The resultant is MoS_2 powders of different shapes. The size of individual particles can be adjusted to some extent. Very frequently, the powders are post-annealed to high temperature, to improve their crystalline quality and purity. The only difference between hydrothermal and solvothermal synthesis is that the precursor solution in the latter case is usually not aqueous. Other solution chemical processes start at around room temperature and atmospheric pressure, where post annealing is often used anyway. The products can be either a powder or thin film, depending on the preparation details. The most commonly-used precursor is (NH4)2MoS4 (ammonium tetrathiomolybdate), or sodium molybdate. (NH4)2MoS_4 decomposes to form MoO3 at 120- 360 °C, [24]which can be further converted into MoS_2.

2.2.3 Characterization:

In this section the characterization techniques that are used in order to analyze the end product formed during the synthesis process and to determine whether the desired results are obtained or not. We discussed different techniques, instrumentations used. Also, how to interpret the raw data/information obtained during analysis to reach to certain conclusions.

Based on the previous works following are the characterization techniques for MoS_2.

(i) Optical Microscopy

(ii) Scanning Electron Microscope (SEM)

(iii) X-Ray Powder Diffraction (XRD)

(iv) X-Ray Photoelectron Spectroscopy (XPS)

(v) Raman Spectroscopy

Know we will discuss about characterizations techniques that were performed to analysis the sample we prepared.

2.3.1 Optical Microscopy:

Reflective light microscopy is the observation of a sample in microscope under a reflective light instead of the conventional transmitting light. As the sample is opaques thus light cannotbe transmitted through it to the eyepiece.

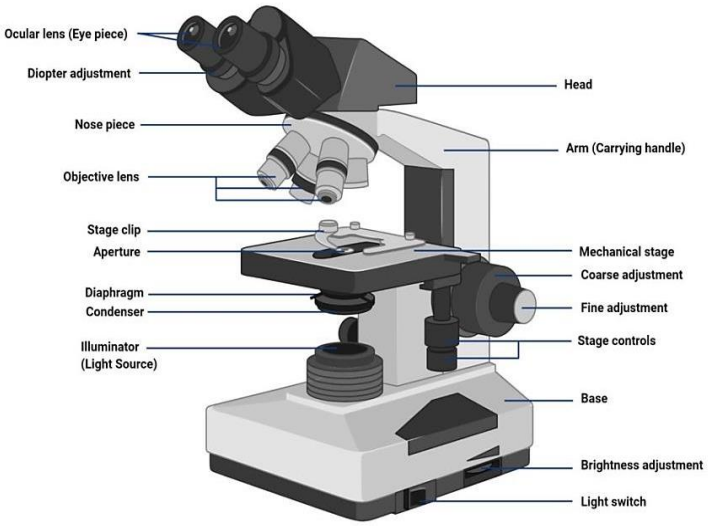

Figure 2.6 Parts of Reflected Light Microscope
Source: www.microbenotes.com

A light microscope uses either transmitted or reflected light for illumination to examine microstructures. Reflective light Source is used for observation of opaque samples. The incidentlight on the surface of the microscope is reflected and observed with eyepiece or mounted camera setup. Based upon the different lenses different level of magnification can be achieved i.e. 10X, 20X, 5X.

2.3.2 Scanning Electron Microscopy (SEM):

Scanning electron microscopy has transformed the way we look at our world. Dimensions considered invisible were now exposed with the advent of this technology. A beam of electron

scans the sample in a manner called raster scanning. The electrons interact in a variety of ways with the sample producing backscattered electrons, Auger electrons, secondary electrons, characteristic X-rays, etc. All these are picked up and analyzed by detectors. SEM is strictly a surface and sub-surface technique reaching up to few nm into the sample. It is highly useful to determine the morphology and chemical composition of sample.

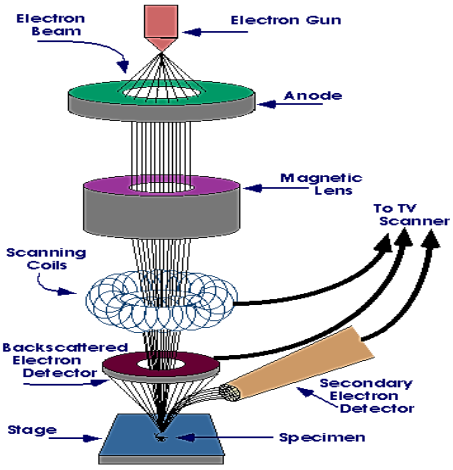

Figure 2.7 Scanning electron microscope.
Source: Radiological and environment

2.3.3 X-Ray Diffraction (XRD):

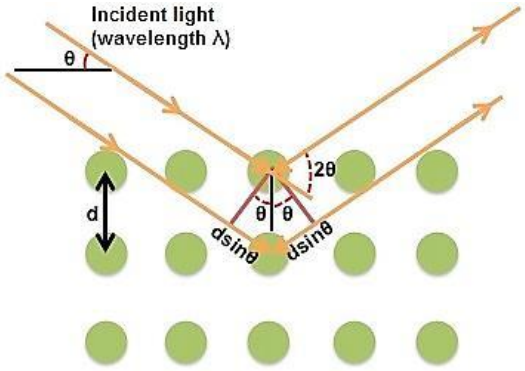

Figure 2.8 XRD pattern formed
Source: https://cnx.org/m

It is a technique used to find the planes (h ,k, l). It is a no destructive characterization.

The monochromatic X-ray beams strikes the powder specimens kept in thin waled capillary. The x ray sore diffracted from specific planes making an angle theta with the beam and obeying Bragg's law. The diffracted rays generate cone concentration with incident beam.

The full opening angle of the diffraction cone 4 theta is determined by measuring the distance S between two diffraction lines corresponding to a particular plane and is related to the Bragg angle by R is specimen to film distance usually the radius of camera housing the film. A list of theta values can be obtained from measuring values if S (Humphreys, 2013).

Where the wave length is λ

$$n\lambda = 2d \sin\theta \qquad (2.1)$$

D is the spacing btw neighboring planes (h, k, l), N is integer.

2.3.4 X-Ray Photoelectron Spectroscopy (XPS):

XPS is quantitative technique for analyzing the elemental composition of the surface of a material. It is also known as electron spectroscopy for chemical analysis. XPS spectra are observed by irradiating a solid with a beam of monochromatic X-rays. Evaluate chemical bonding states (oxidation state) Electronic structure of surface Investigation of growth and reaction of thin films.

XPS analysis is based on the Einstein's Photoelectric effect i.e. emission of particles from thesurface of a material whenever electromagnetic radiation is incident upon it. An X-ray beam comprising K_α is focused on the sample which is absorbed by the surface electron. If the energy of the incident particle is greater than that of binding energy of surface material then electron is ejected from surface. Energy of the photoelectron is measure with thedetector to determine binding energy and other characteristics of the sample.

Binding energy is measured by the following equation

$$K_e = h\nu - B.E - \varphi \qquad (2.2)$$

Where K_e= kinetic energy (measured) ,

φ= work function of spectrometer

$h\nu$ = photon energy from the radiation Source

BE= Binding energy (unknown)

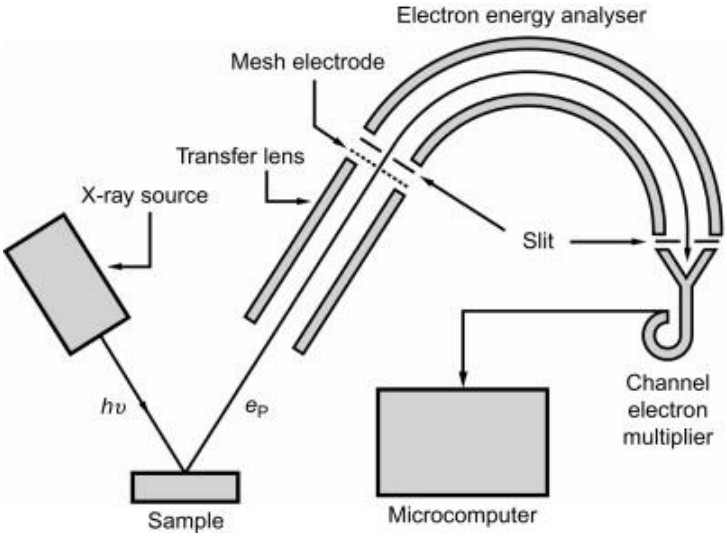

Figure 2.9 Schematic representation of XPS components.
Source: Photoelectron Spectrometer (ESCA) \| Introduction to JEOL Products \| JEOL L

2.3.5 Raman spectroscopy:

Raman spectroscopy's basic principle is Raman Effect .When light strikes a material, some of it is absorbed by the material, while the majority is scattered. Rayleigh scattering is the most common type of scattering in nature. The frequency and energy of scattered light are identical to that of incident light. The least scattered light is inelastically scattered into stokes and anti-stokes, which have different frequencies and energies than incident. The Raman spectrum is made up of inelastic scattered light, and the wavelength-shifted photons are known as Raman scatter. It's known as the N process in phonon terminology.

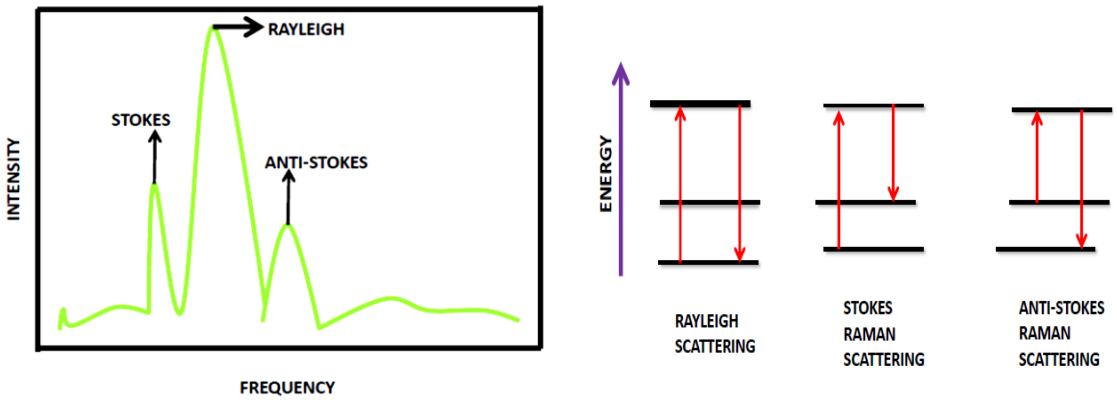

Figure 2.10 Represent a) stokes and anti-stokes, b) Represent energy band diagram for stokes and anti-stokes.

Raman spectrometer is a device which works on principle of Raman scattering. And gives information of intensity verses Raman shift (cm^{-1}). It is type of characterization from which we conclude structure and optical properties of material.

2.3.5.1 Construction and working of Raman spectrometer:

The parts of Raman spectrometer are Source, sample device, monocromator. detector device and modern spectrometer.

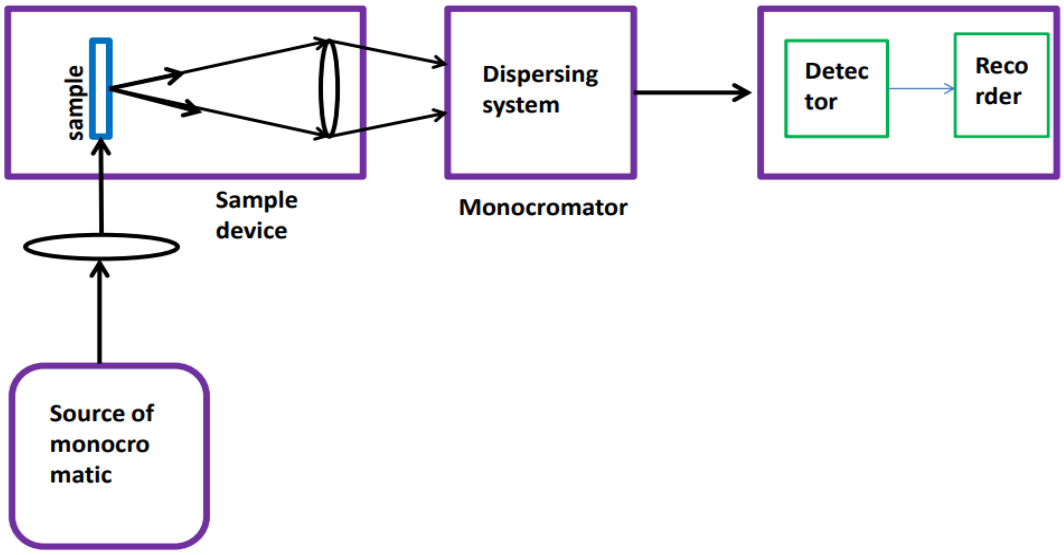

Figure 2.11 Represent block diagram of Raman spectroscopy

Source: Laser is used because they are highly intense and it is good for Raman scattering.eg argon, krypton, He-Ne etc. Intensity of Raman varies as the forth power of frequency.

Chapter-3

Experimental Techniques

Using a thermal CVD, MoS_2 was synthesized on a SiO_2 substrate. To get a better notion of how to proceed with the experiment, a literature evaluation of earlier research studies on the CVD synthesis of monolayer MoS_2 was first conducted.

3.1 Setup of Equipment:

All the management needed for equipment before syntheses are: The quartz tube should be secured in position between the coils. The inlet and outlet in the quartz tube are to be connected to Argon cylinders and rotameters respectively. Care must be taken when handling the quartz tube. MCB's are used to provide a secure electrical connection to the CVD. The CVD that we are using for the synthesis is a dual zone CVD with a high temperature zone and low temperature zone, making it advantageous for vaporization and chemical reaction. As the precursors used have separate melting points.

3.2 Synthesis:

After setting up all the instruments and performing the prerequisites, experiment is started. The CVD used is programmable so the temperature and time periods are preprogrammed with the help of controller and verified for any discrepancies.

3.3 Precondition for synthesis:

All the apparatus and substrates are to be cleaned carefully after setting up equipment.

To avoid form contaminations that can affect the end product and the desired results. The quantity of precursor should be weighed after tearing. Table 3.1 is the set of points done before experimentation takes place. Like cleaning in DI water, acetone, methanol by ultrasonication the substrate (Si or SiO_2) at 50℃ for 5 min to 10 minutes and weighing the precursor's (MoO_3 and S). Using precursor of same company is mandatory.

Table 3.1 Steps before experiment

Steps before experiment	Sub Steps taken
1. Cleaning of substrate in beaker	1) Dipped in methanol at 50C for 5min in ultra-sonicate bath 2) Then in Acetone at 50C for 5min in ultra-sonicate. 3) Then in Deionized (DI) water at 50C for 5 min in ultsonicate.
2. Cleaning Ceramic boat	1) Boats are filled with acetone and then ultrasonicated at 50^{o} C for 5 mins. 2) Boats are filled with methanol and placed in ultrasonication for 5minsat 50^{o} C. 3) Same step as previous with DI water.
3. Cleaning Quartz tube	1) Left out of previous reaction is cleaned from: a) Dusting cloth b) Isopropyl c) Long road
4. Precursors weighing	1) Milligram weighing machine is used. 2) Tear the reading to zero after keeping butter paper. 3) Put precursors in different cleaned ceramic boat.

3.5 Procedure for operating a CVD:

1) A long rod with a curved end for placing the ceramic combustion vessel containing MoO_3 (molybdenum trioxide) and S (Sulphur) powder and Si (silicon) facing down above the high temperature zone (Zone 1) is kept within the quartz tube.
2) The position of ceramic vessel containing S (Sulphur) powder is over the low temperature region (Zone 2).
3) The cotton-based insulator is put at both ends, then screwed on the caps to close the ends.
4) The rotameters are linked at both ends to the quartz tube to monitor and regulate the inert gas flow. The cylinder knob is coupled to the rotameter on the side of Zone 2.
5) CVD is switched on, and the gas flow is tracked throughout the reaction.
6) The gas flow is stopped after the procedure is over and the CVD is turned off .
7) After the CVD gets cooled then substrate is removed for inspection.

3.5 Working Mechanism:

Inert gas (Argon) is flowed through the tube for 15 minutes before to the experiment to maintain a neutral environment. With time, the temperature increases in both zones until it exceeds the melting points of the precursors—115.2 °C for Sulphur and 795 °C for molybdenum trioxide—and then begins to evaporate. The precursors' vapors are conveyed together, where they chemically interact and deposit molybdenum disulfide on the surface of the substrate (SiO_2). The deposition of the product on the substrate layer is facilitated by maintaining a gas flow of 100 sscm and a constant temperature during the deposition period. This cools down even further and coats the substrate surface with a Nano film.

$$MoO_3 + S/2 \rightarrow MoO_3 + 1/2SO_2 \quad (3.3)$$

$$MoO_2 + 3S \rightarrow MoS_2 + SO_2 \quad (3.4)$$

3.6 Experimental Treatments:

1) Quantity for precursors used for MoO_3 and S were from 6-8mg and 300-150mg respectively.
2) The gas flow at the growth period which was for 10min kept at 100-200sscm.

3.7 Outcome & Precautions:

1) After three four attempts we got the best CVD optimization parameters.
2) Optimizing parameters for best outcome are :

Table 4.2 Optimizing parameters with perfect result.

1) Distance between boats	21cm
2) Precursor quantity	MoO3=6mg, S=150mg
3) Growth temperature	MoO3=875C, S=175C
4) Duration of growth period	10min
5) Gas flow	150sscm
6) Placement of substrate	Face down, horizontal and vertical

3.8 Precautions:

1) Laboratory equipment should be handled the proper with security measures.

2) Rubber gloves should be used while cleaning the equipment and substrates as cleaning reagents in direct contact may harm skin. Much attention be given while using strong acidic or basic compounds.

3) Gas flow should be monitored properly at the outlet pipe also as sometimes deposition may lead to block the pipe or hole which can cause the quartz tube to burst and harm anyone nearby.

Chapter 4

Results & Discussion

In this chapter we have discuss the results obtained from the various characterization of the sample synthesized by CVD as discussed in previous chapter 3. We will also discuss the future scope in next chapter.

4.1 Characterization Results:

4.1.1 Optical microscopy:

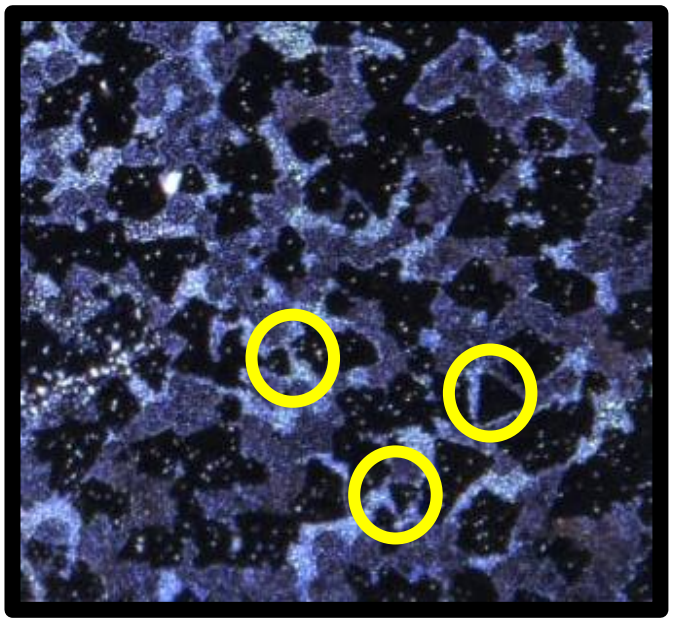

Figure 5.1 Represents optical image and the yellow circled show triangular domains

The sample was observed under an optical microscope illuminated reflected light and images were obtained at 50X optical zoom which was further zoomed digitally using computer applications and as shown in Figure 4.1. Grown flakes are marked with a triangular formed is MoS_2.

4.1.2 SEM (Scanning Electron Microscopy):

SEM tells the morphology of sample formed, and from fig it could be seen that it is of triangular shape. Which confirms that the substance prepared was MoS_2.

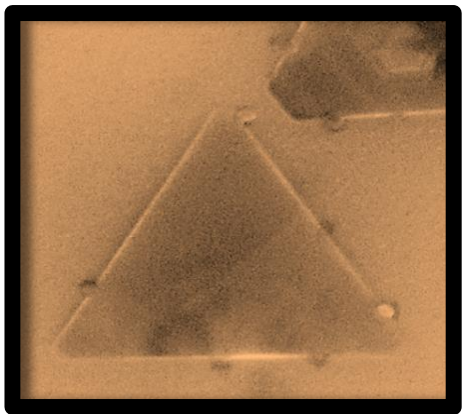

Fig 4.2 Show the triangular domain of sample prepared

4.1.3 X-Ray Diffraction:

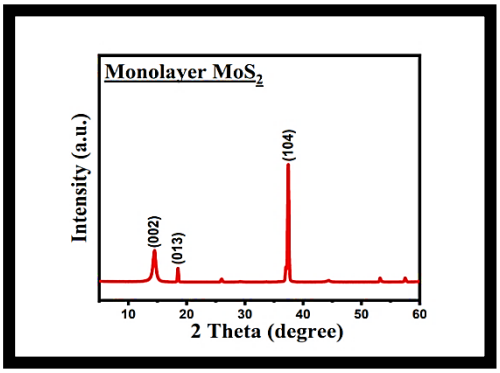

Fig 4.3 Shows Intensity vs 2theta graph plot

XRD data was plotted and was matched with the JCPS. And planes were confirmed at planes (002), (013) and (104), which tells us that it is MoS_2 .We then calculated crystalline size using Scherrer equation $D = 0.9\lambda / \beta \cos\theta$ (1)

Where D is crystalline size, λ is wavelength of X-Ray, β is FWHM and θ is angle between rays.

Crystalline size is 15.9 nm for plane (002)

4.1.4 X-ray Photoelectron Spectroscopy:

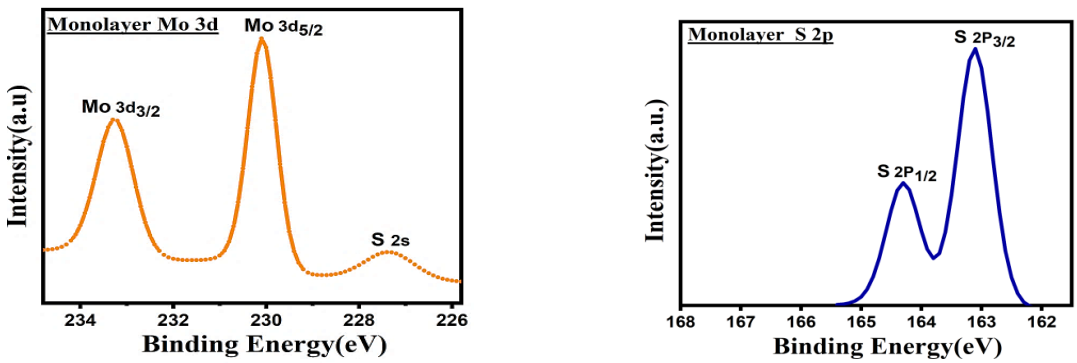

Figure 4.4 Represent Mo intensity verse binding energy. B) S intensity verses B.E

XPS was performed for the Sample and the peaks were observed as shown in Figure 5.1 X-ray Photoelectron Spectroscopy of MoS2: (a) Mo 3d (b) S 2p . The spectra confirm presence of Mo

and S. The peaks were observed at 233.8 eV (MoO_2 $3d_{3/2}$),230.8 eV (MoO_2 $3d_{5/2}$), 227.7eV (S 2s), 224.9 and 165.75 eV (S $2P_{1/2)}$ and 163eV (S $2p_{3/2}$) which is analyzed tallying with the data from NIST X-ray Photoelectron.

4.1.5 Raman Spectroscopy at different temperatures:

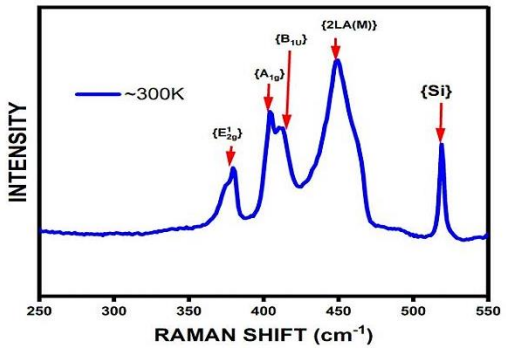

Raman Modes	Raman Shift(cm^{-1})	Raman Intensity	FWHM
E^1_{2g}	384.5745	17005.80	15.3956
A_{1g}	404.941176	23556.02	2.6447
B_{1u}	411.833105	21830.78	6.7348
2LA(M)	449.179207	29594.36	24.9266
Si	519.425445	20105.54	3.57185

Figure 4.5 Showa) Raman spectroscopy at room temperature b) Table 4.1 Raman modes at room temp

The Raman spectra were used to investigate structural properties at various temperatures (198-573K). Raman spectrum acquired at room temperature with a 633 nm laser spanning a wavenumber range of 100–800 cm^{-1} as shown in fig5.5. The difference between A_{1g} and E^1_{2g} peak positions is 20 cm-1 for MoS_2 monolayer and 27 cm-1 for MoS2 bulk, according to literature. Thus, according to our data studying the Raman spectrum with a difference of 20 cm^{-1} between peak of in plane (E^1_{2g}) and out plane (A_{1g}) vibration locations is assigned[26] to MoS_2 monolayer.

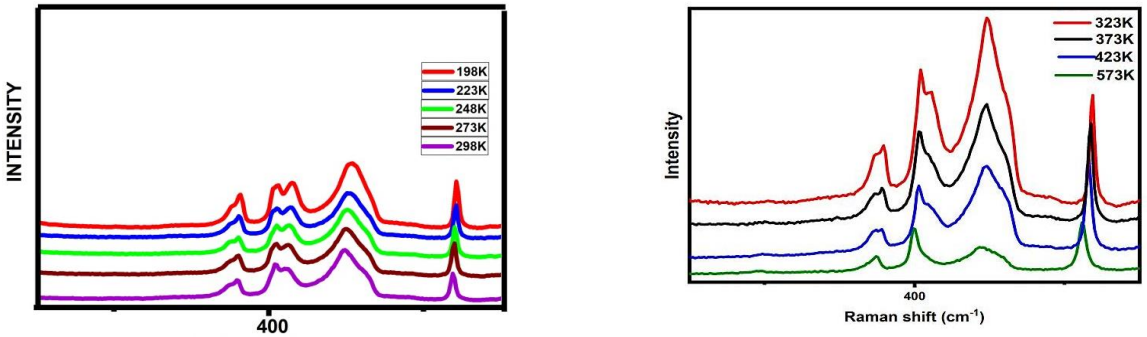

Figure 4.6 a) Raman shift verses intensity below room temperature. b) Above room temperature

Above room temperature data can be seen from table. Where FWHM (Full width at half maxima) is calculated using single peek fit. From table 4.2 for all Raman modes FWHM is increasing and Raman shift is shifting towards lower wave number.

Fig 4.7 was comparing to literature and we concluded that as temperature increase FWHM increasing. FWHM tells us about the life time of phonon, as FWHM increase life time of phonon decreases.[27]

Tabel a) 4.2 data for below room temperature b) above room temperature

Temperature	E^1_{2g}		A_{1g}		Raman shift 2LA(M)
	Raman shift	FWHM	Raman shift	FWHM	
198K	381.825	10.2173	406.0	14.027	453.732
223K	379.224	10.43	405.59	14.719	452.343
248K	378.13	11.842	404.99	12.576	451.317
273K	378.29	11.624	404.95	11.988	450.703
298K	377.61	12.940	404.05	10.608	449.913

Temperature	E^1_{2g}		A_{1g}		Raman shift 2LA(M)
	Raman shift	FWHM	Raman shift	FWHM	
323K	376.3	10.817	404.8	12.24	449.1
373K	378.1	10.988	403.6	14.35	448.2
423K	374.9	11.623	403.8	16.23	448.8
573K	373.7	14.872	399.9	17.47	445.4

5.1 Analysis of Raman Spectroscopy

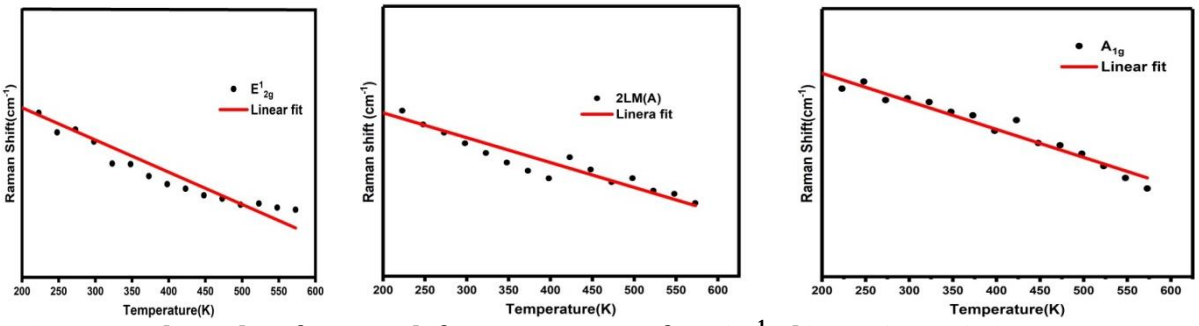

Figure 4.8 show plot of raman shift vs temperature for, a)E^1_{2g} b) A_{1g} c) 2LA(M)

In Fig. 4.8, the change in peak location of the E^1_{2g} , A_{1g} and 2LM(A) modes as a function of temperature is displayed [28]. The following equation was used to match the data of peak position versus temperature:

$$\omega(T)=\omega o+\chi T \qquad (4.1)$$

Where ωo is the E^1_{2g} or A_{1g} modes' vibration frequency at absolute zero temperature,

χ is the E^1_{2g}, A_{1g} or 2LA(M) modes' first order temperature coefficient.[29]

The value is represented by the slope of the fitted straight line. The values for the E^1_{2g}, A_{1g} and 2LA(M) modes, are -0.01808 cm^{-1}/K , -0.01581cm^{-1}/K and -0.01856 cm^{-1}/K respectively.

Chapter- 5

Conclusions and Future Scope

1) MoS_2 was prepared using chemical vapour depostion method.
2) SEM, XRD, XPS, Optical microscopy and raman spectroscopy was done.
3) Raman was studied below and above room temperature .
4) Temperature coefficients for E^1_{2g}, A_{1g} and 2LA(M) are -0.018 cm -1/K , -0.015cm -1/K and -0.018-1/K respectively. Temperature cofficent calculated is negative.
5) Peaks broadens as temperature increase's due to increase in phonon decay. Can be calculated through FWHM of all Raman modes.
6) Raman peak shift towards lower wave number as temperature increase's due to increases in Crystallinity(softening of phonon).
7) With increse in temperature anharmonicity increses.

5.2 Future scope:

Photoelectronic devices of MoS_2 are used due to its tunable band gap, Howerve the performance of a device highly depend on thermal conductivity and structual properaties of the material.thus we studied raman spectrocopy at different temprtatures and caluculated temperature cofficent for diferent raman modes.and they came out to be negative .which tells us that thermal conductivity and electrical resistivty decreses as temperature increse .hence due this property we can use MoS_2 fos Photo electronc devices which will not be affected by temperature.

References

[1] Y. Dong, Z.S. Wu, W. Ren, H.M. Cheng, X. Bao, Graphene: a promising 2D material for electrochemical energy storage, Sci. Bull. 62 (2017) 724–740. https://doi.org/10.1016/j.scib.2017.04.010

[2] C. Biswas, Y.H. Lee, Graphene versus carbon nanotubes in electronic devices, Adv. Funct. Mater. 21 (2011) 3806–3826. https://doi.org/10.1002/adfm.201101241.

[3] X. Li, H. Zhu, Two-dimensional MoS2: Properties, preparation, and applications, J. Mater. 1 (2015) 33–44. https://doi.org/10.1016/j.jmat.2015.03.003.

[4] D. Ma, J. Shi, Q. Ji, K. Chen, J. Yin, Y. Lin, Y. Zhang, M. Liu, Q. Feng, X. Song, X. Guo, J. Zhang, Y. Zhang, Z. Liu, A universal etching-free transfer of MoS2 films for applications in photodetectors, Nano Res. 8 (2015) 3662–3672. https://doi.org/10.1007/s12274-015-0866-z.

[5] X. Zhang, G. Ma, J. Wang, Hydrothermal synthesis of two-dimensional MoS2 and its applications, Tungsten. 1 (2019) 59–79. https://doi.org/10.1007/s42864-019-00014-9.

[6] O. V. Yazyev, A. Kis, MoS2 and semiconductors in the flatland, Mater. Today. 18 (2015) 20–30. https://doi.org/10.1016/j.mattod.2014.07.005.

[7] G.G. Naumis, Electronic properties of two-dimensional materials, INC, 2020. https://doi.org/10.1016/B978-0-12-818475-2.00005-2.

[8] A. Steinhoff, J.H. Kim, F. Jahnke, M. Rösner, D.S. Kim, C. Lee, G.H. Han, M.S. Jeong, T.O. Wehling, C. Gies, Efficient Excitonic Photoluminescence in Direct and Indirect Band Gap Monolayer MoS2, Nano Lett. 15 (2015) 6841–6847. https://doi.org/10.1021/acs.nanolett.5b02719.

[9] S. Jayabal, J. Wu, J. Chen, D. Geng, X. Meng, Metallic 1T-MoS2 nanosheets and their composite materials: Preparation, properties and emerging applications, Mater. Today Energy. 10 (2018) 264–279. https://doi.org/10.1016/j.mtener.2018.10.009.

[10] W. Zhao, J. Pan, Y. Fang, X. Che, D. Wang, K. Bu, F. Huang, Metastable MoS2: Crystal Structure, Electronic Band Structure, Synthetic Approach and Intriguing Physical Properties, Chem. - A Eur. J. 24 (2018) 15942–15954. https://doi.org/10.1002/chem.201801018.

[11] J. Strachan, A.F. Masters, T. Maschmeyer, 3R-MoS2in Review: History, Status, and Outlook, ACS Appl. Energy Mater. 4 (2021) 7405–7418. https://doi.org/10.1021/acsaem.1c00638.

[12] R.M. Arif Khalil, F. Hussain, A. Manzoor Rana, M. Imran, G. Murtaza, Comparative study of

polytype 2H-MoS2 and 3R-MoS2 systems by employing DFT, Phys. E Low-Dimensional Syst. Nanostructures. 106 (2019) 338–345. https://doi.org/10.1016/j.physe.2018.07.003.

[13] N. Bandaru, R.S. Kumar, D. Sneed, O. Tschauner, J. Baker, D. Antonio, S.N. Luo, T. Hartmann, Y. Zhao, R. Venkat, Effect of pressure and temperature on structural stability of MoS 2, J. Phys. Chem. C. 118 (2014) 3230–3235. https://doi.org/10.1021/jp410167k.

[14] P.D. Fleischauer, R. Bauer, Chemical and structural effects on the lubrication properties of sputtered MoS2 films, Tribol. Trans. 31 (1988) 239–250. https://doi.org/10.1080/10402008808981819.

[15] I.A. Rahman, A. Purqon, First Principles Study of Molybdenum Disulfide Electronic Structure, J. Phys. Conf. Ser. 877 (2017). https://doi.org/10.1088/1742-6596/877/1/012026.

[16] A.K.M. Newaz, D. Prasai, J.I. Ziegler, D. Caudel, S. Robinson, R.F. Haglund, K.I. Bolotin, Electrical control of optical properties of monolayer MoS2, Solid State Commun. 155 (2013) 49–52. https://doi.org/10.1016/j.ssc.2012.11.010.

[17] X. Tong, E. Ashalley, F. Lin, H. Li, Z.M. Wang, Advances in MoS2-Based Field Effect Transistors (FETs), Nano-Micro Lett. 7 (2015) 203–218. https://doi.org/10.1007/s40820-015-0034-8.

[18] D. Lee, E. Hwang, Y. Lee, Y. Choi, J.S. Kim, S. Lee, J.H. Cho, Multibit MoS2Photoelectronic Memory with Ultrahigh Sensitivity, Adv. Mater. 28 (2016) 9196–9202. https://doi.org/10.1002/adma.201603571.

[19] A. Savan, E. Pflüger, P. Voumard, A. Schröer, M.S. Paul, Modern solid lubrication: Recent developments and applications of MoS2, Lubr. Sci. 12 (2000) 185–203. https://doi.org/10.1002/ls.3010120206.

[20] E. Akbari, K. Jahanbin, A. Afroozeh, P. Yupapin, Z. Buntat, Brief review of monolayer molybdenum disulfide application in gas sensor, Phys. B Condens. Matter. 545 (2018) 510–518. https://doi.org/10.1016/j.physb.2018.06.033.

[21] K.S. Novoselov, A.H. Castro Neto, Two-dimensional crystals-based heterostructures: Materials with tailored properties, Phys. Scr. 014006 (2012). https://doi.org/10.1088/0031-8949/2012/T146/014006.

[22] A. Raza, J.Z. Hassan, M. Ikram, S. Ali, U. Farooq, Q. Khan, M. Maqbool, Advances in Liquid-Phase and Intercalation Exfoliations of Transition Metal Dichalcogenides to Produce 2D Framework, Adv. Mater. Interfaces. 8 (2021) 1–46. https://doi.org/10.1002/admi.202002205.

[23] Y.A. Kurapov, S. Litvin, N.N. Belyavina, E.I. Oranskaya, S.M. Romanenko, Y. Stelmakh, Synthesis of pure (ligandless) titanium nanoparticles by EB-PVD method, J. Nanoparticle Res. 23 (2021). https://doi.org/10.1007/s11051-020-05110-3.

[24] Y. Peng, Z. Meng, C. Zhong, J. Lu, W. Yu, Z. Yang, Y. Qian, Hydrothermal synthesis of MoS2 and its pressure-related crystallization, J. Solid State Chem. 159 (2001) 170–173. https://doi.org/10.1006/jssc.2001.9146.

[25] M. Mukaida, I. Hiyama, T. Tsunoda, Y. Imai, Preparation of Fe-Si thin films by chemical vapor deposition, Int. Conf. Thermoelectr. ICT, Proc. 9 (1998) 237–240. https://doi.org/10.1109/ict.1998.740360.

[26] X. Li, J. Li, K. Wang, X. Wang, S. Wang, X. Chu, M. Xu, X. Fang, Z. Wei, Y. Zhai, B. Zou, Pressure and temperature-dependent Raman spectra of MoS2 film, Appl. Phys. Lett. 109 (2016). https://doi.org/10.1063/1.4968534.

[27] C. Rani, D.K. Pathak, M. Tanwar, S. Kandpal, T. Ghosh, M.Y. Maximov, R. Kumar, Anharmonicity induced faster decay of hot phonons in rutile TiO2nanorods: A Raman spectromicroscopy study, Mater. Adv. 3 (2022) 1602–1608. https://doi.org/10.1039/d1ma00940k.

[28] X. Huang, Y. Gao, T. Yang, W. Ren, H.M. Cheng, T. Lai, Quantitative Analysis of Temperature Dependence of Raman shift of monolayer WS2, Sci. Rep. 6 (2016) 1–8. https://doi.org/10.1038/srep32236.

[29] S. Sahoo, A.P.S. Gaur, M. Ahmadi, M.J. Guinel, R.S. Katiyar, Temperature Dependent Raman Studies and Thermal Conductivity of Few Layer MoS Temperature Dependent Raman Studies and Thermal Conductivity of Few, (2013). https://doi.org/10.1021/jp402509w.

[30] TWI. What is X-Ray diffraction analysis (XRD) and how does it work? https://www.twi-global.com/technical-knowledge/faqs/x-ray diffraction.

[31] Behera, A.; Mallick, P.; Mohapatra, S. S. Nanocoatings for Anticorrosion. In *CorrosionProtection at the Nanoscale*; Elsevier, 2020; pp 227–243. https://doi.org/10.1016/B978-0-12-819359-4.00013-1.

[32] Barua, S.; Geng, X.; Chen, B. Graphene-Based Nanomaterials for Healthcare Applications. In *Photonanotechnology for Therapeutics and Imaging*; Elsevier, 2020; pp 45–81 https://doi.org/10.1016/B978-0-12-817840-9.00003-5.

[33] Madhuri, K. V. Thermal Protection of Metal Oxide Powders. In *Metal Oxide Powder* Elsevier, 2020; pp 209–231.https://doi.org/10.1016/B978-0-12-817505-7.00010-5.

[34] Magda, G. Z.; Petõ, J.; Dobrik, G.; Hwang, C.; Biró, L. P.; Tapasztó, L. Exfoliation of Large-Area Transition Metal Chalcogenide Single Layers. *Sci. Rep.* **2015**, *5*, 3–7. https://doi.org/10.1038/srep14714.

[35] Shi, Y.; Zhang, H.; Chang, W. H.; Shin, H. S.; Li, L. J. Synthesis and Structure of Two-Dimensional Transition-Metal Dichalcogenides. *MRS Bull.* **2015**, *40* (7), 566–576. https://doi.org/10.1557/mrs.2015.121.

[36] Sun, J.; Li, X.; Guo, W.; Zhao, M.; Fan, X.; Dong, Y.; Xu, C.; Deng, J.; Fu, Y. Synthesis Methods of Two-Dimensional MoS2: A Brief Review. *Crystals* **2017**, *7* (7), 1–11. https://doi.org/10.3390/cryst7070198.

[37] Makhlouf, A. S. H. *Current and Advanced Coating Technologies for Industria Appl* Woodhead Publishing Limited,2011.https://doi.org/10.1533/9780857094902.1.3.

[38]Hiremath, N.; Bhat, G. *High-Performance Carbon Nanofibers and Nanotubes*; 2017. https://doi.org/10.1016/B978-0-08-100550-7.00004-8.

[39] Hoang, A. T.; Qu, K.; Chen, X.; Ahn, J. H. Large-Area Synthesis of Transition Metal Dichalcogenides: Via CVD and Solution-Based Approaches and Their Device Applications. *Nanoscale* **2021**, *13* (2), 615–633. https://doi.org/10.1039/d0nr08071c.

[40] TWI. What is X-Ray diffraction analysis (XRD) and how does it work? https://www.twi- global.com/technical-knowledge/faqs/x-ray-diffraction.

[41] Dutrow, B.; Lousiana State University; Clark, C.; Estern Michigan University. *X- PS*

[42] Murthy, A. P., Theerthagiri, J., Madhavan, J., & Murugan, K. (2017). Highly active MoS2/carbon electrocatalysts for the hydrogen evolution reaction - Insight into the effect of the internal resistance and roughness factor on the Tafel slope. Physical Chemistry Chemical Physics, 19(3), 1988–1998. https://doi.org/10.1039/c6cp07416b

[43] Newbury, D. E. (2009). Mistakes encountered during automatic peak identification of minor and trace constituents in electron-excited energy dispersive X-ray microanalysis. Scanning, 31(3), 91–101. https://doi.org/10.1002/sca.20151

[44] Novoselov, K. S., & Castro Neto, A. H. (2012). Two-dimensional crystals-based heterostructures: Materials with tailored properties. Physica Scripta, T146. https://doi.org/10.1088/0031-8949/2012/T146/014006

[45] O'Brien, M. (2017). Synthesis and raman characterisation of transition metal dichalcogenides. March. Orava, J., Kohoutek, T., & Wagner, T. (2013). DepositionTechniques for chalcogenide thinfilms. https://doi.org/10.1533/9780857093561.1.265

[46] Raman, C. V., & Krishnan, K. S. (1928). A new type of secondary radiation. Nature, 121(3048), 501–502. https://doi.org/10.1038/121501c0

[47] Sanchez-Herencia, A. J. (2007). Water Based Colloidal Processing of Ceramic Laminates. Key Engineering Materials, 333, 39–48. https://doi.org/10.4028/www.scientific.net/kem.333.39

[48] Scriven, L. E. (1988). Physics and Applications of DIP Coating and Spin Coating. MRS Proceedings, 121, 717–729. https://doi.org/10.1557/proc-121-717

[49] Shi, Y., Huang, J. K., Jin, L., Hsu, Y. Te, Yu, S. F., Li, L. J., & Yang, H. Y. (2013). Selective nanoparticles on monolayer MoS_2 single crystals. Scientific Reports, 3, 1–7. https://doi.org/10.1038/srep01839

[50] Splendiani, A., Sun, L., Zhang, Y., Li, T., Kim, J., Chim, C. Y., Galli, G., & Wang, F. (2010). Emerging photoluminescence in monolayer MoS2. Nano Letters, 10(4), 1271–1275. https://doi.org/10.1021/nl903868w

[51] Sun, J., Li, X., Guo, W., Zhao, M., Fan, X., Dong, Y., Xu, C., Deng, J., & Fu, Y. (2017). Synthesis methods of two-dimensional MoS2: A brief review. Crystals, 7(7), 1–11 https://doi.org/10.3390/cryst707